

# Low-Toxicity Perovskite Applications

Subjects: Engineering, Electrical & Electronic

Contributor: Maria Bidikoudi

Perovskite solar cells (PSCs) with earth-abundant carbon as an effective replacer for unstable hole transporting materials and expensive electrodes is a recently proposed structure promising better air and moisture stability.

Keywords: lead-free perovskites ; carbon electrode ; perovskite solar cells ; HTL-free

---

## 1. Introduction

Perovskites, which are materials with the crystal structure similar to calcium titanium oxide ( $\text{CaTiO}_3$ ), were first discovered in 1839, when the Russian mineralogist L. A. Perovski discovered the mineral  $\text{CaTiO}_3$ . However, it was not until the late 1990s, when the structural dynamics of methylammonium lead iodide perovskite ( $\text{MAPbI}_3$ ) material were studied and explored for application in optoelectronics, such as thin-film transistors, photovoltaics (PV) and light-emitting diodes [1][2]. Since then, huge leaps of progress have been made and perovskites have been implemented in high-performing solar cells [3], light-emitting diodes [4], photodetectors [5], lasers [6], as well as sensors, fuel cells, superconductors, catalysis and more [7][8].

The greatest progress and the most intensive research have been towards the application of perovskites as absorbers for solar energy conversion applications. In that direction, perovskite solar cells (PSCs) have achieved power conversion efficiencies (PCEs) that are now comparable with the traditional, well-established and widely applied technology of Si solar cells. Among the different perovskite structures, the perovskite of the organic-inorganic metal halide (OIH) group are the ones that systematically achieve the highest PCEs that are being reported. However, even though PSCs count more than 10 years of extensive study and optimizations, there is still a gap towards the commercialization of this technology. This barrier is mainly caused by three factors: (i) the reduction of PCE when moving to large area devices, (ii) the questionable stability of PSCs under real-life working conditions and (iii) the toxicity of the starting materials, most of all the lead (Pb) content.

For the up scaling of PSCs, a lot of effort has been invested in the device engineering and construction methods, which has led to large area devices with PCEs exceeding 15% [9][10]. The sources of perovskite instability include, among others, water and moisture degradation, thermal stress, light and oxygen induced degradation, ion migration and corrosion of the back contact [11]. One of the most efficient and promising methods to overcome these problems, originating from the corrosion of the metal electrode, is turning it into a different type of PSC: Carbon electrode-based Perovskite Solar Cells (C-PSCs).

In a typical structure, PSCs comprise of a multilayered device architecture of the absorber "sandwiched" between an electron transport layer (ETL) and a hole transport layer (HTL), while the circuit is completed by a metal back electrode, most commonly Au or Ag. During the long-term operation of PSCs, the migration of iodine and metals, combined with the formation of metal halide ions and oxygen vacancies, start to corrode the metal electrode, leaving the structure exposed to the environment and causing a slow degradation [12][13]. In C-PSCs, the metal electrode is replaced by a carbon (C) electrode. Carbon has an appropriate work function ( $W_F$ ) of  $-5$  eV to qualify for an efficient charge collector, while at the same time its hydrophobic nature repels oxygen and moisture from the ambient, providing a protective barrier for the perovskite layer. At the same time the inertness of C allows to remain unaffected by ion migration. This has enabled devices with long-term stability to be achieved, without the need for encapsulation [14].

Being on a track with significant advances in the aspect of overcoming the two out of three barriers which hinder the commercialization of PSCs, the remaining obstacle that needs to be tackled is the environmental and health issues caused by the toxicity of Pb and other perovskite precursor components, such as the HTL and perovskite additives. The European Union has imposed strict rules on the use of toxic elements in consumer electronics. If this problem is not resolved, the PSC technology is bound to remain in lab scale and research level. Hence, the last years have seen lots of efforts for the partial or total elimination of Pb, and its substitution by other metals, which are less toxic and

environmentally and health friendly. Most of the research has been focused on the typical metal electrode structure PSCs, since it is the one that exhibits the highest PCEs so far; however, with the continuous rise of C-PSCs and their additional advantage of stability and significantly lower cost than the metal electrode PSCs, it is prominent that there needs to be a turn to low-toxicity materials' implementation in C-PSCs as well.

## 2. Carbon-Based Perovskite Solar Cells (C-PSCs)

### 2.1. General Description

Carbon-based perovskite solar cells (C-PSCs) differ from the traditional structures in that the metal electrode is eliminated, replaced by a carbon electrode typically prepared using simple methods, such as doctor blading, screen printing and painting, by a C paste. Depending on the temperature that is required for the annealing of the C paste, in order for the electrode to form, they can be distinguished in two main categories: high-temperature (HT) and low-temperature (LT) C-PSCs. Both structures have the same working principle: upon illumination, excitons are produced by the perovskite absorbing layer, forming free charge carriers (electrons and holes); electrons are drawn to the electron transport layer (ETL) and holes are collected from the hole transport layer (HTL). The C electrode, having an appropriate work function ( $W_F$ ), similar to Au, and Fermi level above the valence band edge of the perovskite, can draw the carriers to the external circuit. Moreover, carbon has the capability to absorb oxygen and moisture, thus protecting the perovskite and providing highly stable devices. Even though the initial reports of C-PSCs achieved PCEs much lower than the conventional devices, typically below 10%, the intensive research in this field has led to optimized devices with comparable PCEs to the high-performing metal electrode PSCs, with higher stability and at a significantly lower cost (Figure 1).

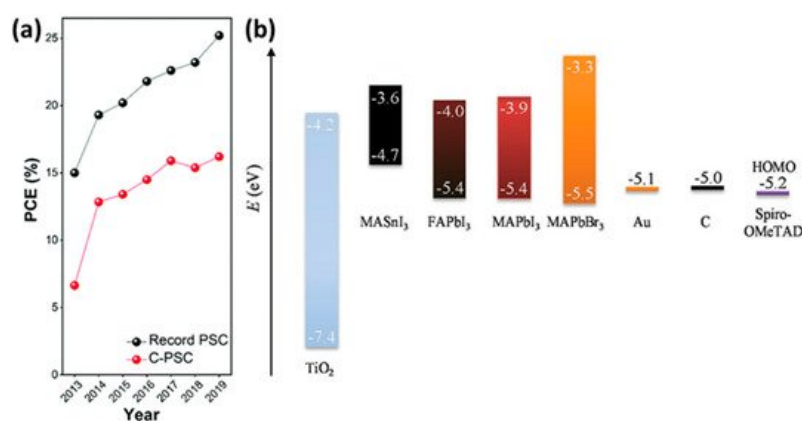


**Figure 1.** (a) Summary of development in PCEs of C-PSCs in comparison to state-of-the-art PSCs [15]. Reproduced with permission—Copyright 2020 Royal Society of Chemistry. (b) schematic energy level diagram of perovskite materials, TiO<sub>2</sub>, Spiro-OMeTAD, Au and C [16]. Reproduced with permission—Copyright 2017 Wiley-VCH.

### 2.2. High-Temperature (HT) C-PSCs

The representative HT device configuration comprises of multiple oxide layers on top of which the perovskite is deposited and formed after annealing. In particular, a compact hole blocking layer, typically TiO<sub>2</sub> or SnO<sub>2</sub> grown from precursor solutions, is first deposited on FTO glass substrates, to minimize recombination losses and prevent shunting pathways. Next, an Electron Transport Layer (ETL) is deposited, which is most commonly the wide bandgap semiconductor Titanium Dioxide (TiO<sub>2</sub>) in a mesoporous structure, followed by an additional mesoporous layer, typically ZrO<sub>2</sub> or AlO<sub>3</sub>. This layer acts as a spacer, preventing the direct contact of TiO<sub>2</sub> with the C electrode, which would cause a short circuiting of the device. Finally, the mesoporous C electrode is deposited from a starting C paste, which is then annealed at a high temperature to remove binders and organic substances and increase the conductivity of the resulting electrode. The perovskite precursor solution is then infiltrated through the triple mesoscopic stack and the perovskite film is formed after annealing (Figure 2). This type of devices are also referred to as “monolithic” and additionally to being HTL-free, highly stable and able to be prepared under ambient conditions, they can also be entirely prepared by printing methods, which gives an advantage when moving to up scaling.

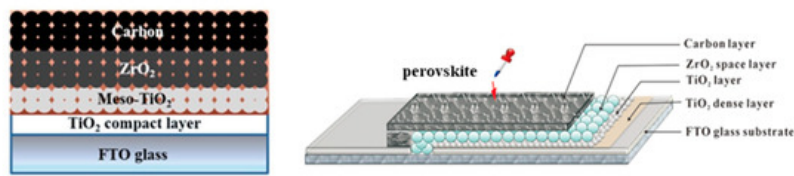


**Figure 2.** A schematic structure of a HT carbon-based “monolithic” perovskite solar cell [17] and the corresponding device illustration [18]. Reproduced with permission—Copyright 2013 Nature Publishing Group.

A variety of carbon materials have been used in order to prepare high-performing C pastes, which would result in C electrodes of high conductivity, low series resistance and great mechanical stability. Among these, the combination of carbon black (CB) and graphite has been established as a high-performing formulation [18][19][20][21], while carbon nanotubes (CNTs) have also shown promising results [22][23]. In all of the highest-performing HT C-PSCs the perovskite formulations that have been used are Pb-based, with the most common being the  $AVA_xMA_{(1-x)}PbI_3$ , while recently efforts have turned to the incorporation of multiple cation structures, for the enhancement of performance and stability (Table 1). In the typical HT C-PSC structure, no HTL is employed; however, the state of the art PSCs of this structure have achieved PCE of 17%, when a Nickel Oxide (NiO) layer has been employed as the HTL [24], combined with a mixed cation-mixed halide perovskite (Figure 3).

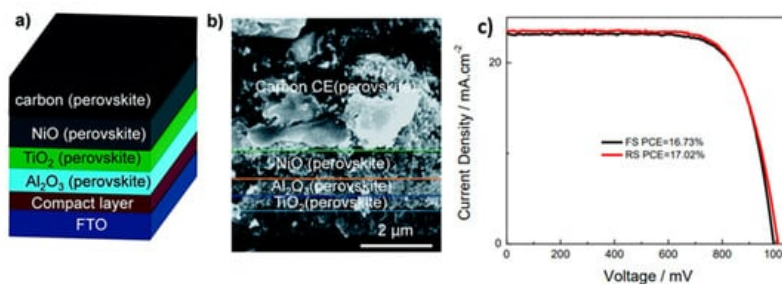


**Figure 3.** (a) Schematic architecture of the C-PSC consisting of FTO glass as a transparent substrate, a compact  $TiO_2$  layer, a mesoporous  $TiO_2$  layer, an  $Al_2O_3$  layer and NiO layer coated with graphite/carbon black CE; (b) cross section SEM image of device with  $TiO_2/Al_2O_3/NiO/C$  ( $CS_x(FA_{0.4}MA_{0.6})_{1-x}PbI_{2.8}Br_{0.2}$ ) structure; (c) J-V curves of champion perovskite solar cell devices under standard AM 1.5G illumination at  $100\text{ mWcm}^{-2}$  [24]. Reproduced with permission—Copyright 2017 Royal Society of Chemistry.

**Table 1.** Summary table of some of the highest-performing HT C-PSCs that have been reported so far.

PCE (%)	Perovskite	HTL	Device Configuration	Carbon Paste Formulation	Year/Reference	Comments
17.02	$CS_{0.05}(FA_{0.4}MA_{0.6})_{0.95}PbI_{2.8}Br_{0.2}$	NiO	FTO/c- $TiO_2$ /mp- $TiO_2/Al_2O_3/NiO/C$	Graphite/carbon black	2017 [24]	sequential deposition
16.51	$(5-AVA)_x(MA)_{1-x}PbI_3$	-	FTO/c- $TiO_2$ /mp- $TiO_2/ZrO_2/C$	Commercial C paste	2020 [25]	PBS-X; X = Li, Na, and K post treatment of $TiO_2/ZrO_2/C$
16.37	$MAPbI_3$	-	FTO/c- $TiO_2$ /mp- $TiO_2/PbTiO_3/CNTs$	CNTs sprayed	2019 [23]	ultrathin layer of ferroelectric $PbTiO_3$ on the $TiO_2$ scaffold
16.26	$CS_{0.1}Rb_{0.05}FA_{0.85}PbI_3$	-	FTO/c- $TiO_2$ /mp- $TiO_2/ZrO_2/C$	Carbon/spheroidal graphite	2019 [26]	1. DMF:DMSO: Formamide mixed solvent 2. Evaporation control
15.9	$CH_3NH_3PbI_3(SrCl_2)_x$	-	FTO/c- $TiO_2$ /mp- $TiO_2/Al_2O_3/C$	Graphite/ carbon black	2016 [27]	$SrCl_2$ chemical modification of perovskite
15.77	$(5-AVA)_x(MA)_{1-x}PbI_3$	-	FTO/c- $TiO_2$ /mp- $TiO_2/ZrO_2/C$	carbon black/graphite	2019 [28]	VOx post-treatment of C/perovskite interface

PCE (%)	Perovskite	HTL	Device Configuration	Carbon Paste Formulation	Year/Reference	Comments
15.7	$(5\text{-AVA})_x(\text{MA})_{(1-x)}\text{PbI}_3$	-	FTO/c-TiO <sub>2</sub> /mp-TiO <sub>2</sub> /ZrO <sub>2</sub> /C	Graphite/ carbon black	2018 [29]	oxygen-rich carbon black
15.6	CH <sub>3</sub> NH <sub>3</sub> PbI <sub>3</sub>	-	FTO/c-TiO <sub>2</sub> /mp-TiO <sub>2</sub> /ZrO <sub>2</sub> /C	Carbon/spheroidal graphite	2017 [30]	1. additive of ammonium chloride (NH <sub>4</sub> Cl) 2. Two-step process during perovskite formation
15.6	AB-MAPbI <sub>3</sub>	-	FTO/c-TiO <sub>2</sub> /mp-TiO <sub>2</sub> /ZrO <sub>2</sub> /C	Graphite/ carbon black	2017 [31]	1. 4-(aminomethyl) benzoic acid hydroiodide (AB) organic cation 2. benzylamine hydroiodide (BA) benzylamine hydroiodide (BA) organic cation 3. 5-AVAI organic cation
15.11	$(5\text{-AVA})_x(\text{MA})_{1-x}\text{PbI}_3$	-	FTO/c-TiO <sub>2</sub> /mp-TiO <sub>2</sub> /ZrO <sub>2</sub> /C	Graphite/ carbon black	2019 [32]	1. Ethanol co-solvent in GBL
15.03	CH <sub>3</sub> NH <sub>3</sub> PbI <sub>3</sub>	NiO	FTO/c-TiO <sub>2</sub> /mp-TiO <sub>2</sub> /Al <sub>2</sub> O <sub>3</sub> /NiO/C	Graphite/ carbon black	2015 [33]	quadruple-layer architecture
15	CH <sub>3</sub> NH <sub>3</sub> PbI <sub>3</sub>	-	FTO/c-TiO <sub>2</sub> /mp-TiO <sub>2</sub> /Al <sub>2</sub> O <sub>3</sub> /C	Graphite/ carbon black	2017 [34]	1. NMP solvent 2. slow crystallization (SC) method
15	Cs <sub>0.1</sub> FA <sub>0.9</sub> PbI <sub>3</sub>	-	FTO/c-TiO <sub>2</sub> /mp-TiO <sub>2</sub> /ZrO <sub>2</sub> /C	Commercial C paste	2019 [35]	Prepared in glove box
14.9	CH <sub>3</sub> NH <sub>3</sub> PbI <sub>3</sub>	NiO	FTO/c-TiO <sub>2</sub> /mp-TiO <sub>2</sub> /ZrO <sub>2</sub> /NiO/C	Graphite/ carbon black	2015 [36]	sequential deposition
14.7	CH <sub>3</sub> NH <sub>3</sub> PbI <sub>3</sub>	-	FTO/c-TiO <sub>2</sub> /mp-TiO <sub>2</sub> /Al <sub>2</sub> O <sub>3</sub> /C	SWCNTs/carbon black	2016 [22]	SWCNT-doped graphite/carbon black electrode
14.5	MAPbI <sub>3-x</sub> Cl <sub>x</sub>	-	FTO/c-TiO <sub>2</sub> /mp-TiO <sub>2</sub> /ZrO <sub>2</sub> /C	Carbon/spheroidal graphite	2018 [37]	Addition of 0.45M MACI increases PCE from 8.74% to 14.5%
14.5	CH <sub>3</sub> NH <sub>3</sub> PbI <sub>3</sub>	-	FTO/c-TiO <sub>2</sub> /mp-TiO <sub>2</sub> /ZrO <sub>2</sub> /C	N/A	2016 [38]	Effect of LiCl additive
14.3	$(5\text{-AVA})_x(\text{MA})_{(1-x)}\text{PbI}_3$	-	FTO/c-TiO <sub>2</sub> /mp-TiO <sub>2</sub> /ZrO <sub>2</sub> /C	Commercial C paste	2017 [39]	humidity assisted thermal exposure (HTE) as a post-treatment method—150 h
14.27	CH <sub>3</sub> NH <sub>3</sub> PbI <sub>3-x</sub> GuCl	-	FTO/c-TiO <sub>2</sub> /mp-TiO <sub>2</sub> /ZrO <sub>2</sub> /C	Commercial C paste	2016 [40]	1. Additive GuCl in perovskite 2. Voc 1.02V
14.2	CH <sub>3</sub> NH <sub>3</sub> I	NiO	FTO/c-TiO <sub>2</sub> /mp-TiO <sub>2</sub> /ZrO <sub>2</sub> /NiO/C	carbon black/graphite	2015 [41]	1. NiO nanosheet paste on ZrO <sub>2</sub> 2. Comparison of nanoparticles and nanosheets. 3. Screen printed device

### 2.3. Low-Temperature (LT) C-PSCs

The low-temperature C-PSC configuration, besides the obvious difference of the C paste requiring a low-temperature annealing to form the C electrode, differs from the HT in two major aspects: (a) the C electrode is deposited after the perovskite deposition and crystallization on the appropriate substrate and (b) the mesoporous layers can be omitted and replaced by planar ones. Particularly for the spacer layer, this can be entirely eliminated, since the perovskite layer intervenes between the C electrode and the ETL, thus preventing a short circuit at this interface. This type of devices are also referred to as “paintable” (Figure 4).

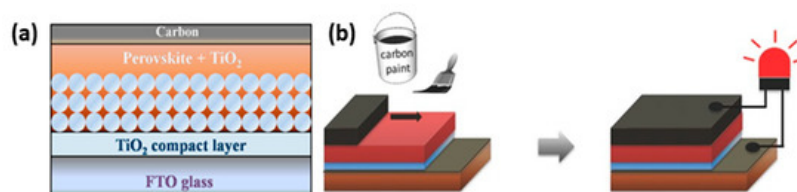


**Figure 4.** (a) Schematic illustrating the cell architecture [42]. Reprinted with permission from Zhang, F.; Yang, X.; Wang, H.; Cheng, M.; Zhao, J.; Sun, L. *ACS Appl. Mater. Interfaces* **2014**, *6*, 16140–16146-Copyright 2014 American Chemical Society and (b) fabrication process of LT “paintable” perovskite solar cells [43]. Reproduced with permission—Copyright 2016 Wiley-VCH.

The carbon pastes that are being used typically consist of carbon black, graphite, polymer, additive and a non-polar solvent. In this type of C-PSC, it is crucial that the components of the paste are compatible with the underlying perovskite layer, in order to avoid its decomposition. It is noteworthy that this architecture benefits the use of free-standing electrodes as well as electrodes that are simply press transferred on the perovskite layer, giving the opportunity for high efficiency devices with an ease of fabrication and an extremely low cost [44][45][46][47]. Additionally, in this structure the perovskite is grown directly on the ETL, avoiding the infiltration through multiple mesoporous layers. This gives a much higher flexibility and a variety of choices for the perovskite structures to be used. This has led to devices with PCEs comparable to the ones of Au-based devices, owing to the potential of multiple cation, multiple halide perovskites for high-performance and high-stability devices, as summarized in Table 2. The current state-of-the-art LT C-PSC has achieved PCE of 19.2%, in devices with self-standing C films used as counter electrode, mixed cation perovskite structure and spiro-OMeTAD as the HTM [44] (Figure 5).

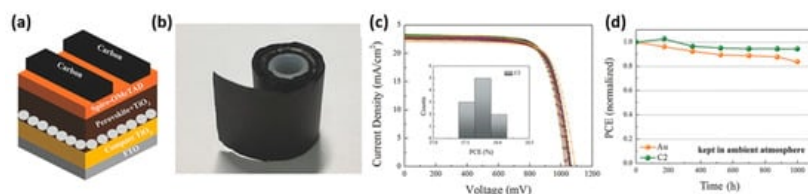


**Figure 5.** (a) Schematic diagram of C-PSCs; (b) the roll-up of C films; (c) Uniform performance of devices based on C films rolled up for a week; (d) stability test of C-PSCs kept in ambient atmosphere without any encapsulation [44]. Reproduced with permission—Copyright 2018 Wiley-VCH.

**Table 2.** Summary table of some of the highest-performing LT C-PSCs that have been reported so far.

PCE (%)	Perovskite	HTL	Device Configuration	Carbon Paste Formulation	Year/Reference	Comments
19.2	$(\text{FA}_{0.75}\text{MA}_{0.25})\text{PbI}_{2.75}\text{Br}_{0.25}$	spiro-OMeTAD	FTO/c-TiO <sub>2</sub> /mp-TiO <sub>2</sub> /perovskite/spiro-OMeTAD/C	Commercial C paste	2018 [44]	self-standing films
18.65	$\text{Cs}_{0.05}(\text{MA}_{0.17}\text{FA}_{0.83})_{0.95}\text{Pb}(\text{I}_{0.83}\text{Br}_{0.17})_3$	spiro-OMeTAD	FTO/c-TiO <sub>2</sub> /mp-TiO <sub>2</sub> /perovskite/spiro-OMeTAD/C	Graphene in IPA	2019 [48]	various commercial carbon sources (carbon black, graphite sheet, and graphene) studied
18.22	$\text{FA}_{0.3}\text{MA}_{0.7}\text{PbI}_3$	P3HT/graphene	FTO/SnO <sub>2</sub> @TiO <sub>2</sub> /perovskite/P3HT/C	C in propylene glycol monomethyl ether acetate	2019 [49]	Stability 89% of original PCE after 600 h
18.1	$(\text{FA}_{0.83}\text{MA}_{0.17})\text{PbI}_{2.15}\text{Br}_{0.85}$	CuSCN	FTO/c-TiO <sub>2</sub> /mp-TiO <sub>2</sub> /perovskite/CuSCN/C	graphitic carbon layer	2019 [50]	≈95% of their initial efficiencies for >2000 h under full-sun illumination

PCE (%)	Perovskite	HTL	Device Configuration	Carbon Paste Formulation	Year/Reference	Comments
17.78	$\text{Cs}_{0.05}(\text{MA}_{0.17}\text{FA}_{0.83})_{0.95}\text{Pb}(\text{I}_{0.83}\text{Br}_{0.17})_3$	CuPc	FTO/Zn:SnO <sub>2</sub> /perovskite/CuPc/C	Commercial C paste	2019 [51]	Zn-doped SnO <sub>2</sub> ETL
17.58	$\text{Cs}_{0.05}(\text{FA}_{0.83}\text{MA}_{0.17})_{0.95}\text{Pb}(\text{I}_{0.83}\text{Br}_{0.17})_3$	CuSCN	FTO/c-TiO <sub>2</sub> /mp-TiO <sub>2</sub> /perovskite/CuSCN/C	MWCNTs in chlorobenzene	2019 [52]	1. MWCNTs to replace carbon black 2. Stability 80% after 1000 h 1 sun illumination
17.56	FACsPbI <sub>3</sub>	spiro-OMeTAD	ITO/SnO <sub>2</sub> /perovskite/spiro-OMeTAD/C	free-standing CNT sheet	2018 [46]	Trifluoromethanesulfonic acid vapor doping of the free-standing CNT sheet enabled tuning of conductivity and work function of electrode
17.46	$\text{Cs}_{0.05}(\text{FA}_{0.4}\text{MA}_{0.6})_{0.95}\text{Pb}(\text{I}_{2.8}\text{Br}_{0.2})$	CuPc	FTO/Ni:TiO <sub>2</sub> /perovskite/CuPc/C	Commercial C paste	2018 [53]	1. planar 2. Ni-doped rutile TiO <sub>2</sub> as electron transport layer
17.02	$\text{Cs}_{0.05}(\text{FA}_{0.85}\text{MA}_{0.15})_{0.95}\text{Pb}(\text{I}_{0.85}\text{Br}_{0.15})_3$	spiro-OMeTAD	FTO/SnO <sub>2</sub> /perovskite/spiro-OMeTAD/C	Self-adhesive carbon film	2020 [45]	1. planar 2. graphite paper/carbon film electrode
16.6	$\text{Cs}_{0.05}(\text{MA}_{0.17}\text{FA}_{0.83})_{0.95}\text{Pb}(\text{I}_{0.83}\text{Br}_{0.17})_3$	spiro-OMeTAD	FTO/c-TiO <sub>2</sub> /m-TiO <sub>2</sub> /perovskite/C	SWCNT film	2017 [54]	1. press-transferred single-walled carbon nanotube (SWCNT) film infiltrated with Spiro-OMeTAD 2. superior long-term stability at elevated temperatures
16.25	$\text{FA}_x\text{MA}_{1-x}\text{PbI}_y\text{Br}_{3-y}$	-	ITO/SnO <sub>2</sub> /MWCNTs:perovskite/C	Commercial C paste	2019 [55]	1. MWCNTs additive in the perovskite solution 2. all air processed 3. stability 93% under ambient air conditions for 22 weeks
16.2	MAPbI <sub>3</sub> :MAPbI <sub>x</sub> Br <sub>3-x</sub>	-	FTO/c-TiO <sub>2</sub> /m-TiO <sub>2</sub> /perovskite/C	Commercial C paste	2019 [56]	MAPbI <sub>3</sub> /MAPbI <sub>x</sub> Br <sub>3-x</sub> perovskite stacking structure
16.1	MAPbI <sub>3</sub>	CuPc	FTO/c-TiO <sub>2</sub> /m-TiO <sub>2</sub> /perovskite/CuPc/Carbon	Commercial C paste	2016 [57]	8.5% drop during 600 h durability tests
16.03	MAPbI <sub>3</sub>	-	ITO/HMB:C <sub>60</sub> /perovskite/C	Commercial C paste	2019 [58]	1. hexamethonium bromide-doped fullerene C60 ETL 2. No hysteresis
15.73	CH <sub>3</sub> NH <sub>3</sub> PbI <sub>3</sub> -SWCNT	-	FTO/c-TiO <sub>2</sub> /m-TiO <sub>2</sub> /perovskite/SWCNT-C	flaky graphite/spheroidal graphite/ carbon black	2019 [59]	1. SWCNTs in both antisolvent and C electrode 2. stability of 90 days in dark under high humidity and high-temperature conditions
15.6	$\text{Cs}_{0.05}\text{MA}_{0.16}\text{FA}_{0.79}\text{Pb}(\text{I}_{0.84}\text{Br}_{0.16})_3$	-	FTO/c-TiO <sub>2</sub> /m-TiO <sub>2</sub> /perovskite/PEA <sub>2</sub> PbI <sub>4</sub> /C	Commercial C paste	2018 [60]	1. 2D perovskite interlayer 2. Stability 92% of initial PCE after 1000 h of exposure to ambient conditions
15.38	MAPbI <sub>3</sub>	-	FTO/C <sub>60</sub> /perovskite/C	Commercial C paste	2018 [61]	1. First report on fullerene ETL 2. Additional replacement of FTO with graphene based TC electrode
15.29	$\text{Cs}_{0.04}(\text{MA}_{0.17}\text{FA}_{0.83})_{0.96}\text{Pb}(\text{I}_{0.83}\text{Br}_{0.17})_3$	spiro-OMeTAD	FTO/c-TiO <sub>2</sub> /m-TiO <sub>2</sub> /perovskite/C+spiro-OMeTAD	Commercial C paste	2016 [62]	Carbon cloth embedded in C paste electrode

As the interest in C-PSCs is rising, so are the PCE values that are achieved and C-PSCs have now been established as the most promising structure for large-area applications and potential commercialization of perovskite solar modules, owing to their high stability, capability to be processed entirely under ambient conditions, the ability to be HTL-free and, most importantly, their significantly lower cost compared to PSCs with metal electrodes. Hence, it is expected that more progress will be presented in the near years to come. One of the most challenging tasks will be to implement environmentally friendly perovskite structures in C-PSCs, in order to overcome the additional barrier of PSCs towards their commercialization, which are the toxicity issues caused by the Pb content of the perovskite.

## 3. Perovskites

### 3.1. General Description-Current State of the Art

Hybrid organic-inorganic lead halide perovskites are compounds with the general chemical formula ABX<sub>3</sub> and octahedral structure. A is the component that generally forms the unit cell and is an organic monocation, typically CH<sub>3</sub>NH<sub>3</sub><sup>+</sup> (methylammonium-MA), HC(NH<sub>2</sub>)<sub>2</sub><sup>+</sup> (formamidinium-FA) or the inorganic cesium (Cs<sup>+</sup>). Component B is a, smaller than A,

Efficiency (%)	Perovskite	HTL	Device Configuration	Counter Electrode	Formulation	Year/Reference	Comments
15.27	MAPbI <sub>3</sub> :MA <sub>1-x</sub> Cs <sub>x</sub> PbI <sub>3</sub>	-	FTO/c-TiO <sub>2</sub> /m-TiO <sub>2</sub> /perovskite/C	Graphite/carbon black		2020 [63]	Post treatment with acetate salts (CsAc, FAAc, MAAC, KAc, NaAc)
15.23	MAPbI <sub>3</sub>		FTO/c-TiO <sub>2</sub> /m-TiO <sub>2</sub> /m-Al <sub>2</sub> O <sub>3</sub> /perovskite/C	MWCNTs in chlorobenzene		2017 [64]	Boron doping of MWCNTs for enhanced hole extraction

**Figure 6.** The ABX<sub>3</sub> perovskite crystal structure and the atomic structure of three A site cations explored. B is Pb or Sn, and X is a halogen ion [65]. Reproduced with permission—Copyright 2014 Royal Society of Chemistry. On the right side the energy level diagram, showing the processes occurring during a PSC of the normal structure operation is depicted.

Organic-inorganic hybrid perovskites possess optoelectronic properties that make them suitable for applications as photoactive materials in solar cells. These features include high absorptivity, high charge carrier mobility, long exciton diffusion length, tunable bandgap and low exciton binding energy. The CH<sub>3</sub>NH<sub>3</sub>PbI<sub>3</sub> and CH<sub>3</sub>NH<sub>3</sub>PbBr<sub>3</sub> perovskites were first studied and presented as sensitizers in Dye Sensitized Solar Cells (DSSCs) which demonstrated moderate PCE of 3.81% [66]. After that, device engineering, materials composition and chemical modifications have enabled PCEs to rise rapidly and reach 25.5% in 2021 [67], 12 years after their first appearance in the solar cell community. The highest-performing devices, exhibiting PCEs that exceed 20%, employ MA and/or FA as the A cation and Pb as the B cation. Even though the performance of the perovskite based SCs is now comparable in terms of efficiency and stability with Si SCs, at the same time with a much lower cost, there is a major issue towards the commercialization and real-life application of this technology that needs to be tackled, and this is the toxicity and environmental harmfulness of Pb. Especially in consumer electrical and electronic equipment, the use of hazardous materials is prohibited and considering that Pb has been identified as one of the ten hazardous chemicals listed by ROHS in order to avoid its exposure to environment and people, it is mandatory that its use is limited [68][69] (Figure 7). Thus, Pb-based perovskites are unlikely to see a broad industrialization in order to compete with other photovoltaic technologies, unless there is turn to lead-free perovskite materials that would provide stable devices with acceptable PCEs, without endangering the human health and the environment [70].

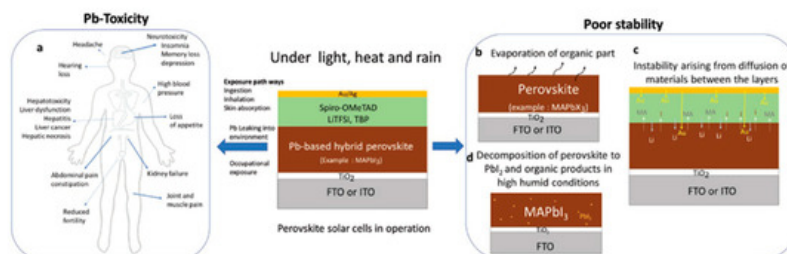


**Figure 7.** Schematic illustration of (a) effect of exposure of toxic-lead on human life and (b–d) factors responsible for the perovskite degradation [71]. Reproduced with permission—Copyright 2019 Wiley-VCH.

Towards that direction, the most promising candidates that have been investigated as substitutes of Pb are Tin (Sn), Germanium (Ge), Bismuth (Bi), Antimony (Sb) and Copper (Cu).

- Tin (Sn)

Tin is considered to be the most suitable candidate for Pb substitution, because of its similar valence electronic configuration and ionic radius ( $\text{Sn}^{2+} = 115 \text{ pm}$  and  $\text{Pb}^{2+} = 119 \text{ pm}$ ) [72]. Sn-based perovskites have the general formula of  $\text{ASnX}_3$ , A being  $\text{MA}^+$ ,  $\text{FA}^+$  or  $\text{Cs}^+$  cation, and X a halogen anion. They have optical bandgap of 1.2–1.6 eV which is appropriate for light absorbing applications and are characterized by large carrier mobilities and low exciton binding energies [73]. The highest PCEs obtained with Sn-based perovskites is 13.24% in an ITO/PEDOT:PSS/perovskite/C60/BCP/Ag device configuration, with the  $(\text{FA}_{1-x}\text{EA}_x)_{0.98}\text{EDA}_{0.01}\text{SnI}_3$  perovskite and 12.96% in a c-TiO<sub>2</sub>/absorber/spiro-OMeTAD/Au, with CsSnI<sub>3</sub> perovskite quantum rods [74][75] (Figure 8).

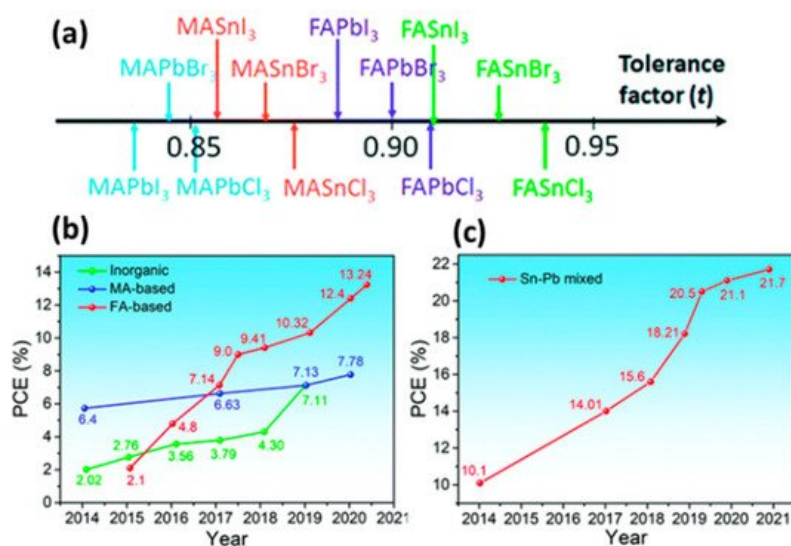


**Figure 8.** (a) Tolerance factor of a series of common perovskites [76] Reprinted with permission—Copyright 2015 Royal Society of Chemistry; Efficiency progress of (b) Sn-based and (c) low-bandgap Sn–Pb mixed PSCs [77]. Reproduced with permission—Copyright 2021 Royal Society of Chemistry.

- Germanium (Ge)

Germanium is another element with valence electronic configuration similar to  $Pb_2^+$ , that qualifies as a potential substitute for low-toxicity PSCs. The ionic radius is 73 pm, which is smaller than Pb and Sn and it possesses analogous electronegativity with Sn; however, it gets more easily oxidized, which makes its handling demanding [70]. The most promising candidates for Ge-based PSCs are ammonium halides ( $AGeX_3$ ), such as methylammonium germanium triiodide ( $MAGeI_3$ ), and cesium germanium triiodide ( $CsGeI_3$ ), owing to their suitable optical bandgap of 1.9 and 1.6 eV, respectively, combined with excellent hole and electron conducting behavior and better stability in ambient conditions than  $MAPbI_3$  [78][79]. The PCEs obtained so far with Ge-based perovskites in PSCs still lay below 1%, in particular 0.57% with  $MAGeI_{2.7}Br_{0.3}$  [80]; however, a PCE of 7.11% has been reported in a mixed Sn–Ge perovskite,  $CsSn_{0.5}Ge_{0.5}I_3$ , and the FTO/PCBM/perovskite/spiro-OMeTAD/Au device structure [81] (Figure 9).

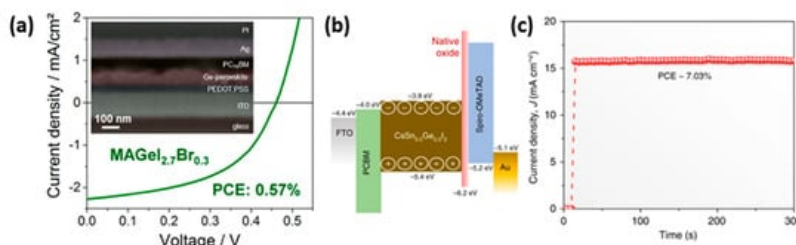


**Figure 9.** (a) SEM image of a FIB processed cross-section and J–V curve of an optimized  $MAGeI_{2.7}Br_{0.3}$  based solar cell [80] Reprinted with permission from Kopacic, I.; Friesenbichler, B.; Hoefler, S.F.; Kunert, B.; Plank, H.; Rath, T.; Trimmel, G. *ACS Appl. Energy Mater.* **2018**, *1*, 343–347—Copyright 2018 American Chemical Society; (b) energy-level diagram of the mixed Sn–Ge perovskite based device and (c) stabilized power output of the Sn–Ge PSC [81]. Reproduced with permission from Chen, M.; Ju, M.-G.; Garcés, H.F.; Carl, A.D.; Ono, L.K.; Hawash, Z.; Zhang, Y.; Shen, T.; Qi, Y.; Grimm, R.L.; et al. *Nat. Commun.* **2019**, *10*, 16—Copyright 2019 Springer Nature.

- Bismuth (Bi)

Bismuth materials (Bi), with the structure of  $A_3Bi_2X_9$  have also drawn significant attention as non-toxic substitutes for Pb, because of their similar electronic configuration, very close ionic radius of 103 pm ( $Pb = 119$  pm) and a good value of electronegativity. They typically consist of A cations of  $MA^+$ ,  $Cs^+$ ,  $Rb^+$ ,  $K^+$ , guanidinium, cyclohexylammonium or imidazolium to form a 0D perovskite structure [82]. The highest PCE recorder so far is of the order of 3.59%, in a  $Cs_3Bi_2I_9$ – $Ag_3Bi_2I_9$  bulk heterojunction (BHJ) perovskite solar cell (Figure 10).

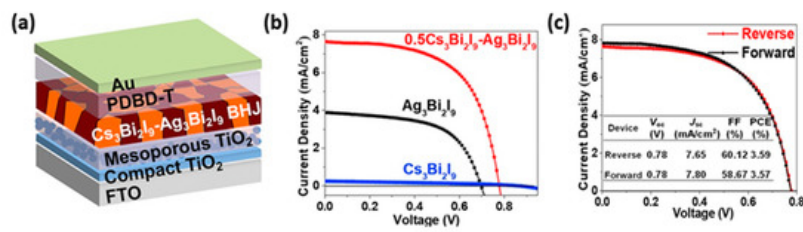


**Figure 10.** (a) Schematic structure of FTO/c-TiO<sub>2</sub>/mp-TiO<sub>2</sub>/photoactive film/PDBD-T/Au device; (b) J-V curves of the champion devices based on different photoactive films; (c) J-V curves of the devices based on 0.5Cs<sub>3</sub>Bi<sub>2</sub>I<sub>9</sub>-Ag<sub>3</sub>Bi<sub>2</sub>I<sub>9</sub> blend films [83]. Adapted with permission—Copyright 2020 Elsevier.

- Antimony (Sb)

Following Bi, antimony (Sb) based perovskites have been evaluated as photoactive materials, since they also exhibit appropriate optoelectronic properties to qualify as efficient absorbers for PSCs. They have the general structure of A<sub>3</sub>Sb<sub>2</sub>X<sub>9</sub>, A being an organic or inorganic cation and X a halogen, while the cation and anion species combination determines the structure and dimensions. The antimony cation has a similar valence electronic configuration with Pb, even though it appears in a trivalent state; therefore, it might exhibit long carrier lifetimes. When incorporated in PSCs, Sb-based perovskites have so far achieved low PCEs, the highest being 3.34%, in a FTO/TiO<sub>2</sub>/perovskite/spiro-OMeTAD/Au device configuration, using the MA<sub>3</sub>Sb<sub>2</sub>I<sub>9-x</sub>Cl<sub>x</sub> perovskite. The PSCs retain 90% of the initial PCE after being stored under ambient conditions for over 1400 h and additionally, semitransparent Sb-based PSCs have been demonstrated with PCEs from 2.62 to 3.06% indicating the great potential for building integrated applications [84] (Figure 11).

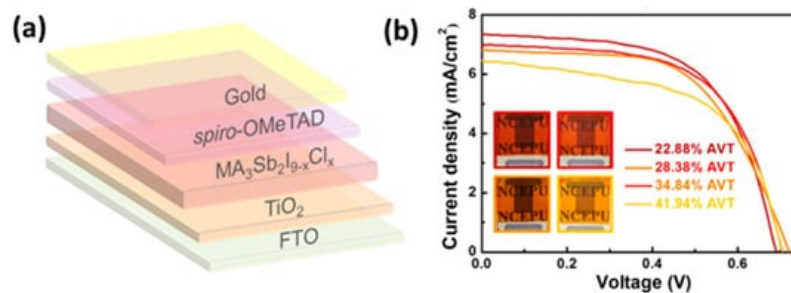


**Figure 11.** (a) Schematic drawing of the semitransparent device architecture of glass/FTO/c-TiO<sub>2</sub>/mp-TiO<sub>2</sub>/MA<sub>3</sub>Sb<sub>2</sub>I<sub>9-x</sub>Cl<sub>x</sub>/spiro-OMeTAD/Au; (b) J-V curves of the semitransparent PSCs with different full-device AVTs, obtained using ~20 nm Au electrodes. The insets are photographs of the as-fabricated semitransparent PSCs (Reprinted with permission from Yang, Y.; Liu, C.; Cai, M.; Liao, Y.; Ding, Y.; Ma, S.; Liu, X.; Guli, M.; Dai, S.; Nazeeruddin, M.K. *ACS Appl. Mater. Interfaces* **2020**, *12*, 17062–17069, Copyright 2020, American Chemical Society) [84].

- Copper (Cu)

Finally, copper (Cu), has also emerged as promising for photovoltaic applications. Because of the small ionic radius (73 pm), layered 2D perovskite structures can be formed, with general formula (RNH<sub>3</sub>)<sub>2</sub>CuX<sub>4</sub> where RNH<sub>3</sub><sup>+</sup> is an aliphatic or aromatic cation and X is a halogen. The highest PCE obtained so far is 2.41%, in a FTO/TiO<sub>2</sub>/perovskite /Spiro-OMeTAD/Au device configuration and (CH<sub>3</sub>NH<sub>3</sub>)<sub>2</sub>CuCl<sub>4</sub> perovskite [85] (Figure 12).

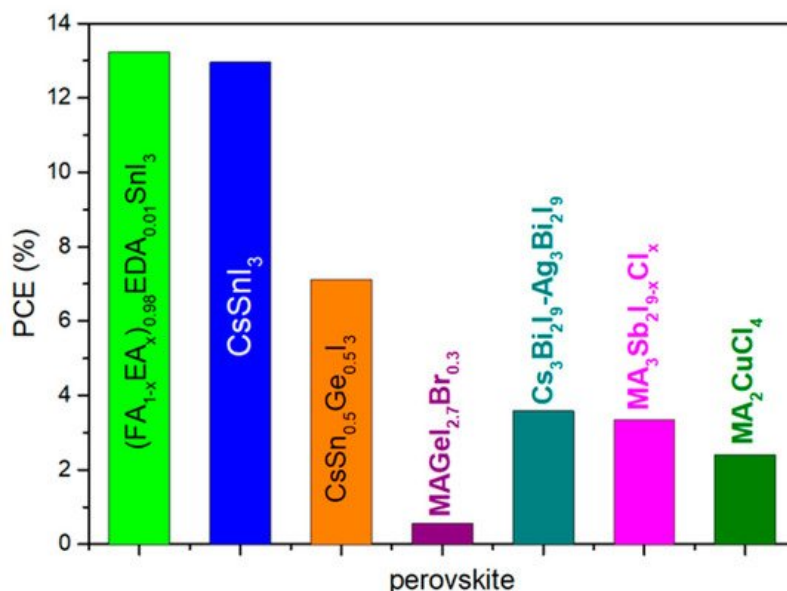


**Figure 12.** Summary of the highest reported PCE of Pb-free perovskites applied in PSCs with metal back contact.

## References

- Mitzi, D.B. Templating and structural engineering in organic–inorganic perovskites. *J. Chem. Soc. Dalton Trans.* 2001, 1–12.
- Mitzi, D.B. Synthesis, Structure, and Properties of Organic-Inorganic Perovskites and Related Materials. *Prog. Inorg. Chem.* 1999, 48, 1–121.
- Best Research-Cell Efficiency Chart. Available online: (accessed on 9 May 2021).
- Bidikoudi, M.; Fresta, E.; Costa, R.D. White perovskite based lighting devices. *Chem. Commun.* 2018, 54, 8150–8169.
- Miao, J.; Zhang, F. Recent progress on highly sensitive perovskite photodetectors. *J. Mater. Chem. C* 2019, 7, 1741–1791.
- Stylianakis, M.M.; Maksudov, T.; Panagiotopoulos, A.; Kakavelakis, G.; Petridis, K. Inorganic and Hybrid Perovskite Based Laser Devices: A Review. *Materials* 2019, 12, 859.
- Atta, N.F. *Perovskite Nanomaterials—Synthesis, Characterization, and Applications*; Galal, A., Ed.; IntechOpen: Rijeka, Croatia, 2016.
- Takano, Y.; Kimishima, Y.; Taketomi, H.; Ogawa, S.; Takayanagi, S.; Mōri, N. New Copper-Free Layered Perovskite Superconductors:  $KCa_2Nb_3O_{10}$  and Related Compounds BT—Stripes and Related Phenomena; Bianconi, A., Saini, N.L., Eds.; Springer: Boston, MA, USA, 2000; pp. 573–578. ISBN 978-0-306-47100-1.
- Park, N.-G.; Zhu, K. Scalable fabrication and coating methods for perovskite solar cells and solar modules. *Nat. Rev. Mater.* 2020, 5, 333–350.
- Zhao, Y.; Ma, F.; Gao, F.; Yin, Z.; Zhang, X.; You, J. Research progress in large-area perovskite solar cells. *Photonics Res.* 2020, 8, A1–A15.
- Wali, Q.; Iftikhar, F.J.; Khan, M.E.; Ullah, A.; Iqbal, Y.; Jose, R. Advances in stability of perovskite solar cells. *Org. Electron.* 2020, 78, 105590.
- Berhe, T.A.; Su, W.-N.; Chen, C.-H.; Pan, C.-J.; Cheng, J.-H.; Chen, H.-M.; Tsai, M.-C.; Chen, L.-Y.; Dubale, A.A.; Hwang, B.-J. Organometal halide perovskite solar cells: Degradation and stability. *Energy Environ. Sci.* 2016, 9, 323–356.
- Wang, J.; Chen, X.; Jiang, F.; Luo, Q.; Zhang, L.; Tan, M.; Xie, M.; Li, Y.-Q.; Zhou, Y.; Su, W.; et al. Electrochemical Corrosion of Ag Electrode in the Silver Grid Electrode-Based Flexible Perovskite Solar Cells and the Suppression Method. *Sol. RRL* 2018, 2, 1800118.
- Grancini, G.; Roldán-Carmona, C.; Zimmermann, I.; Mosconi, E.; Lee, X.; Martineau, D.; Nabey, S.; Oswald, F.; De Angelis, F.; Graetzel, M.; et al. One-Year stable perovskite solar cells by 2D/3D interface engineering. *Nat. Commun.* 2017, 8, 1–8.

15. Hadadian, M.; Smått, J.-H.; Correa-Baena, J.-P. The role of carbon-based materials in enhancing the stability of perovskite solar cells. *Energy Environ. Sci.* 2020, 13, 1377–1407.
16. Chen, H.; Yang, S. Carbon-Based Perovskite Solar Cells without Hole Transport Materials: The Front Runner to the Market? *Adv. Mater.* 2017, 29, 1603994.
17. Cai, Y.; Liang, L.; Gao, P. Promise of commercialization: Carbon materials for low-cost perovskite solar cells. *Chin. Phys. B* 2018, 27, 018805.
18. Ku, Z.; Rong, Y.; Xu, M.; Liu, T.; Han, H. Full Printable Processed Mesoscopic CH<sub>3</sub>NH<sub>3</sub>PbI<sub>3</sub>/TiO<sub>2</sub> Heterojunction Solar Cells with Carbon Counter Electrode. *Sci. Rep.* 2013, 3, 3132.
19. Chen, J.; Xiong, Y.; Rong, Y.; Mei, A.; Sheng, Y.; Jiang, P.; Hu, Y.; Li, X.; Han, H. Solvent effect on the hole-conductor-free fully printable perovskite solar cells. *Nano Energy* 2016, 27, 130–137.
20. Kim, B.; Ko, S.G.; Sonu, K.S.; Ri, J.H.; Kim, U.C.; Ryu, G. II Effects of Adding PbI<sub>2</sub> on the Performance of Hole-Transport Material-Free Mesoscopic Perovskite Solar Cells with Carbon Electrode. *J. Electron. Mater.* 2018, 47, 6266–6271.
21. Mei, A.; Li, X.; Liu, L.; Ku, Z.; Liu, T.; Rong, Y.; Xu, M.; Hu, M.; Chen, J.; Yang, Y.; et al. A hole-conductor-free, fully printable mesoscopic perovskite solar cell with high stability. *Science* 2014, 345, 295–298.
22. Li, H.; Cao, K.; Cui, J.; Liu, S.; Qiao, X.; Shen, Y.; Wang, M. 14.7% Efficient Mesoscopic Perovskite Solar Cells Using Single Walled Carbon Nanotubes/Carbon Composite Counter Electrodes. *Nanoscale* 2016, 8, 6379–6385.
23. Yang, Y.; Liu, Z.; Ng, W.K.; Zhang, L.; Zhang, H.; Meng, X.; Bai, Y.; Xiao, S.; Zhang, T.; Hu, C.; et al. An Ultrathin Ferroelectric Perovskite Oxide Layer for High-Performance Hole Transport Material Free Carbon Based Halide Perovskite Solar Cells. *Adv. Funct. Mater.* 2019, 29, 1806506.
24. Liu, S.; Huang, W.; Liao, P.; Pootrakulchote, N.; Li, H.; Lu, J.; Li, J.; Huang, F.; Shai, X.; Zhao, X.; et al. 17% efficient printable mesoscopic PIN metal oxide framework perovskite solar cells using cesium-containing triple cation perovskite. *J. Mater. Chem. A* 2017, 5, 22952–22958.
25. Sheng, Y.; Ji, W.; Chu, Y.; Ming, Y.; Mei, A.; Hu, Y.; Rong, Y.; Han, H. Post-Treatment of Mesoporous Scaffolds for Enhanced Photovoltage of Triple-Mesoscopic Perovskite Solar Cells. *Sol. RRL* 2020, 4, 2000185.
26. Wang, Q.; Zhang, W.; Zhang, Z.; Liu, S.; Wu, J.; Guan, Y.; Mei, A.; Rong, Y.; Hu, Y.; Han, H. Crystallization Control of Ternary-Cation Perovskite Absorber in Triple-Mesoscopic Layer for Efficient Solar Cells. *Adv. Energy Mater.* 2020, 10, 1903092.
27. Zhang, H.; Wang, H.; Williams, S.T.; Xiong, D.; Zhang, W.; Chueh, C.-C.; Chen, W.; Jen, A.K.-Y. SrCl<sub>2</sub> Derived Perovskite Facilitating a High Efficiency of 16% in Hole-Conductor-Free Fully Printable Mesoscopic Perovskite Solar Cells. *Adv. Mater.* 2017, 29, 1606608.
28. Li, D.; Tong, C.; Ji, W.; Fu, Z.; Wan, Z.; Huang, Q.; Ming, Y.; Mei, A.; Hu, Y.; Rong, Y.; et al. Vanadium Oxide Post-Treatment for Enhanced Photovoltage of Printable Perovskite Solar Cells. *ACS Sustain. Chem. Eng.* 2019, 7, 2619–2625.
29. Tian, C.; Mei, A.; Zhang, S.; Tian, H.; Liu, S.; Qin, F.; Xiong, Y.; Rong, Y.; Hu, Y.; Zhou, Y.; et al. Oxygen management in carbon electrode for high-performance printable perovskite solar cells. *Nano Energy* 2018, 53, 160–167.
30. Rong, Y.; Hou, X.; Hu, Y.; Mei, A.; Liu, L.; Wang, P.; Han, H. Synergy of ammonium chloride and moisture on perovskite crystallization for efficient printable mesoscopic solar cells. *Nat. Commun.* 2017, 8.
31. Hu, Y.; Zhang, Z.; Mei, A.; Jiang, Y.; Hou, X.; Wang, Q.; Du, K.; Rong, Y.; Zhou, Y.; Xu, G.; et al. Improved Performance of Printable Perovskite Solar Cells with Bifunctional Conjugated Organic Molecule. *Adv. Mater.* 2018, 30, 1705786.
32. Ming, Y.; Xu, M.; Liu, S.; Li, D.; Wang, Q.; Hou, X.; Hu, Y.; Rong, Y.; Han, H. Ethanol stabilized precursors for highly reproducible printable mesoscopic perovskite solar cells. *J. Power Sources* 2019, 424, 261–267.
33. Cao, K.; Zuo, Z.; Cui, J.; Shen, Y.; Moehl, T.; Zakeeruddin, S.M.; Grätzel, M.; Wang, M. Efficient screen printed perovskite solar cells based on mesoscopic TiO<sub>2</sub>/Al<sub>2</sub>O<sub>3</sub>/NiO/carbon architecture. *Nano Energy* 2015, 17, 171–179.
34. Tsai, C.M.; Wu, G.W.; Narra, S.; Chang, H.M.; Mohanta, N.; Wu, H.P.; Wang, C.L.; Diau, E.W.G. Control of preferred orientation with slow crystallization for carbon-based mesoscopic perovskite solar cells attaining efficiency 15%. *J. Mater. Chem. A* 2017, 5, 739–747.
35. Hou, X.; Xu, M.; Tong, C.; Ji, W.; Fu, Z.; Wan, Z.; Hao, F.; Ming, Y.; Liu, S.; Hu, Y.; et al. High performance printable perovskite solar cells based on Cs<sub>0.1</sub>FA<sub>0.9</sub>PbI<sub>3</sub> in mesoporous scaffolds. *J. Power Sources* 2019, 415, 105–111.
36. Xu, X.; Liu, Z.; Zuo, Z.; Zhang, M.; Zhao, Z.; Shen, Y.; Zhou, H.; Chen, Q.; Yang, Y.; Wang, M. Hole Selective NiO Contact for Efficient Perovskite Solar Cells with Carbon Electrode. *Nano Lett.* 2015, 15, 2402–2408.

37. Jiang, H.; Liu, X.; Chai, N.; Huang, F.; Peng, Y.; Zhong, J.; Zhang, Q.; Ku, Z.; Cheng, Y. Alleviate the J–V hysteresis of carbon-based perovskite solar cells via introducing additional methylammonium chloride into MAPbI<sub>3</sub> precursor. *RSC Adv.* 2018, 8, 35157–35161.
38. Sheng, Y.; Hu, Y.; Mei, A.; Jiang, P.; Hou, X.; Duan, M.; Hong, L.; Guan, Y.; Rong, Y.; Xiong, Y.; et al. Enhanced electronic properties in CH<sub>3</sub>NH<sub>3</sub>PbI<sub>3</sub>: Via LiCl mixing for hole-conductor-free printable perovskite solar cells. *J. Mater. Chem. A* 2016, 4, 16731–16736.
39. Hashmi, S.G.; Martineau, D.; Dar, M.I.; Myllymäki, T.T.T.; Sarikka, T.; Ulla, V.; Zakeeruddin, S.M.; Grätzel, M. High performance carbon-based printed perovskite solar cells with humidity assisted thermal treatment. *J. Mater. Chem. A* 2017, 5, 12060–12067.
40. Hou, X.; Hu, Y.; Liu, H.; Mei, A.; Li, X.; Duan, M.; Zhang, G.; Rong, Y.; Han, H. Effect of guanidinium on mesoscopic perovskite solar cells. *J. Mater. Chem. A* 2017, 5, 73–78.
41. Liu, Z.; Zhang, M.; Xu, X.; Cai, F.; Yuan, H.; Bu, L.; Li, W.; Zhu, A.; Zhao, Z.; Wang, M.; et al. NiO nanosheets as efficient top hole transporters for carbon counter electrode based perovskite solar cells. *J. Mater. Chem. A* 2015, 3, 24121–24127.
42. Zhang, F.; Yang, X.; Wang, H.; Cheng, M.; Zhao, J.; Sun, L. Structure engineering of hole-conductor free perovskite-based solar cells with low-temperature-processed commercial carbon paste as cathode. *ACS Appl. Mater. Interfaces* 2014, 6, 16140–16146.
43. Chen, H.; Wei, Z.; He, H.; Zheng, X.; Wong, K.S.; Yang, S. Solvent Engineering Boosts the Efficiency of Paintable Carbon-Based Perovskite Solar Cells to Beyond 14%. *Adv. Energy Mater.* 2016, 6, 1502087.
44. Zhang, H.; Xiao, J.; Shi, J.; Su, H.; Luo, Y.; Li, D.; Wu, H.; Cheng, Y.-B.; Meng, Q. Self-Adhesive Macroporous Carbon Electrodes for Efficient and Stable Perovskite Solar Cells. *Adv. Funct. Mater.* 2018, 28, 1802985.
45. Su, H.; Xiao, J.; Li, Q.; Peng, C.; Zhang, X.; Mao, C.; Yao, Q.; Lu, Y.; Ku, Z.; Zhong, J.; et al. Carbon film electrode based square-centimeter scale planar perovskite solar cells exceeding 17% efficiency. *Mater. Sci. Semicond. Process.* 2020, 107, 104809.
46. Lee, J.-W.; Jeon, I.; Lin, H.-S.; Seo, S.; Han, T.-H.; Anisimov, A.; Kauppinen, E.I.; Matsuo, Y.; Maruyama, S.; Yang, Y. Vapor-Assisted Ex-Situ Doping of Carbon Nanotube toward Efficient and Stable Perovskite Solar Cells. *Nano Lett.* 2019, 19, 2223–2230.
47. Bogachuk, D.; Zouhair, S.; Wojciechowski, K.; Yang, B.; Babu, V.; Wagner, L.; Xu, B.; Lim, J.; Mastroianni, S.; Pettersson, H.; et al. Low-temperature carbon-based electrodes in perovskite solar cells. *Energy Environ. Sci.* 2020, 13, 3880–3916.
48. Zhang, C.; Wang, S.; Zhang, H.; Feng, Y.; Tian, W.; Yan, Y.; Bian, J.; Wang, Y.; Jin, S.; Zakeeruddin, S.M.; et al. Efficient stable graphene-based perovskite solar cells with high flexibility in device assembling via modular architecture design. *Energy Environ. Sci.* 2019, 12, 3585–3594.
49. Chu, Q.-Q.; Ding, B.; Peng, J.; Shen, H.; Li, X.; Liu, Y.; Li, C.-X.; Li, C.-J.; Yang, G.-J.; White, T.P.; et al. Highly stable carbon-based perovskite solar cell with a record efficiency of over 18% via hole transport engineering. *J. Mater. Sci. Technol.* 2019, 35, 987–993.
50. Arora, N.; Dar, M.I.; Akin, S.; Uchida, R.; Baumeler, T.; Liu, Y.; Zakeeruddin, S.M.; Grätzel, M. Low-Cost and Highly Efficient Carbon-Based Perovskite Solar Cells Exhibiting Excellent Long-Term Operational and UV Stability. *Small* 2019, 15, 1904746.
51. Ye, H.; Liu, Z.; Liu, X.; Sun, B.; Tan, X.; Tu, Y.; Shi, T.; Tang, Z.; Liao, G. 17.78% efficient low-temperature carbon-based planar perovskite solar cells using Zn-doped SnO<sub>2</sub> electron transport layer. *Appl. Surf. Sci.* 2019, 478, 417–425.
52. Wu, X.; Xie, L.; Lin, K.; Lu, J.; Wang, K.; Feng, W.; Fan, B.; Yin, P.; Wei, Z. Efficient and stable carbon-based perovskite solar cells enabled by the inorganic interface of CuSCN and carbon nanotubes. *J. Mater. Chem. A* 2019, 7, 12236–12243.
53. Liu, X.; Liu, Z.; Sun, B.; Tan, X.; Ye, H.; Tu, Y.; Shi, T.; Tang, Z.; Liao, G. 17.46% efficient and highly stable carbon-based planar perovskite solar cells employing Ni-doped rutile TiO<sub>2</sub> as electron transport layer. *Nano Energy* 2018, 50, 201–211.
54. Kerttu, A.; Konrad, D.; Juan-Pablo, C.; Kári, S.; Michael, S.; Antonio, A.; Michael, G.; Esko, K.; Johansson, J.E.M.; Wolfgang, T.; et al. High Temperature-Stable Perovskite Solar Cell Based on Low-Cost Carbon Nanotube Hole Contact. *Adv. Mater.* 2017, 29, 1606398.
55. Zhou, J.; Wu, J.; Li, N.; Li, X.; Zheng, Y.-Z.; Tao, X. Efficient all-air processed mixed cation carbon-based perovskite solar cells with ultra-high stability. *J. Mater. Chem. A* 2019, 7, 17594–17603.

56. Liu, J.; Zhou, Q.; Thein, N.K.; Tian, L.; Jia, D.; Johansson, E.M.J.; Zhang, X. In situ growth of perovskite stacking layers for high-efficiency carbon-based hole conductor free perovskite solar cells. *J. Mater. Chem. A* 2019, 7, 13777–13786.
57. Zhang, F.; Yang, X.; Cheng, M.; Wang, W.; Sun, L. Boosting the efficiency and the stability of low cost perovskite solar cells by using CuPc nanorods as hole transport material and carbon as counter electrode. *Nano Energy* 2016, 20, 108–116.
58. Zhou, J.; Hou, J.; Tao, X.; Meng, X.; Yang, S. Solution-processed electron transport layer of n-doped fullerene for efficient and stable all carbon based perovskite solar cells. *J. Mater. Chem. A* 2019, 7, 7710–7716.
59. Wang, Y.; Zhao, H.; Mei, Y.; Liu, H.; Wang, S.; Li, X. Carbon Nanotube Bridging Method for Hole Transport Layer-Free Paintable Carbon-Based Perovskite Solar Cells. *ACS Appl. Mater. Interfaces* 2019, 11, 916–923.
60. Lee, K.; Kim, J.; Yu, H.; Lee, J.W.; Yoon, C.-M.; Kim, S.K.; Jang, J. A highly stable and efficient carbon electrode-based perovskite solar cell achieved via interfacial growth of 2D PEA<sub>2</sub>PbI<sub>4</sub> perovskite. *J. Mater. Chem. A* 2018, 6, 24560–24568.
61. Meng, X.; Zhou, J.; Hou, J.; Tao, X.; Cheung, S.H.; So, S.K.; Yang, S. Versatility of Carbon Enables All Carbon Based Perovskite Solar Cells to Achieve High Efficiency and High Stability. *Adv. Mater.* 2018, 30, 1706975.
62. Gholipour, S.; Correa-Baena, J.-P.; Domanski, K.; Matsui, T.; Steier, L.; Giordano, F.; Tajabadi, F.; Tress, W.; Saliba, M.; Abate, A.; et al. Highly Efficient and Stable Perovskite Solar Cells based on a Low-Cost Carbon Cloth. *Adv. Energy Mater.* 2016, 6, 1601116.
63. Liu, T.; Wang, Z.; Lou, L.; Xiao, S.; Zheng, S.; Yang, S. Interfacial Post-Treatment for Enhancing the Performance of Printable Carbon-Based Perovskite Solar Cells. *Sol. RRL* 2020, 4, 1900278.
64. Zheng, X.; Chen, H.; Li, Q.; Yang, Y.; Wei, Z.; Bai, Y.; Qiu, Y.; Zhou, D.; Wong, K.S.; Yang, S. Boron Doping of Multiwalled Carbon Nanotubes Significantly Enhances Hole Extraction in Carbon-Based Perovskite Solar Cells. *Nano Lett.* 2017, 17, 2496–2505.
65. Eperon, G.E.; Stranks, S.D.; Menelaou, C.; Johnston, M.B.; Herz, L.M.; Snaith, H.J. Formamidinium lead trihalide: A broadly tunable perovskite for efficient planar heterojunction solar cells. *Energy Environ. Sci.* 2014, 7, 982–988.
66. Kojima, A.; Teshima, K.; Shirai, Y.; Miyasaka, T. Organometal Halide Perovskites as Visible-Light Sensitizers for Photovoltaic Cells. *J. Am. Chem. Soc.* 2009, 131, 6050–6051.
67. Tandem Solar Cells with High Power Conversion Efficiency. Available online: (accessed on 11 May 2021).
68. World Health Organization Exposure to Lead: A Major Public Health Concern. 2010. Available online: (accessed on 30 April 2021).
69. Wolman, A. Public health and environment. *Am. J. Public Health* 1985, 75, 1049–1051.
70. Kour, R.; Arya, S.; Verma, S.; Gupta, J.; Bandhoria, P.; Bharti, V.; Datt, R.; Gupta, V. Potential Substitutes for Replacement of Lead in Perovskite Solar Cells: A Review. *Glob. Chall.* 2019, 3, 1900050.
71. Miyasaka, T.; Kulkarni, A.; Kim, G.M.; Öz, S.; Jena, A.K. Perovskite Solar Cells: Can We Go Organic-Free, Lead-Free, and Dopant-Free? *Adv. Energy Mater.* 2020, 10, 1902500.
72. Hoefler, S.F.; Trimmel, G.; Rath, T. Progress on lead-free metal halide perovskites for photovoltaic applications: A review. *Monatshefte Chem.* 2017, 148, 795–826.
73. Huang, L.; Lambrecht, W.R.L. Electronic band structure, phonons, and exciton binding energies of halide perovskites CsSnCl<sub>3</sub>, CsSnBr<sub>3</sub>, and CsSnI<sub>3</sub>. *Phys. Rev. B* 2013, 88, 165203.
74. Nishimura, K.; Kamarudin, M.A.; Hirotsu, D.; Hamada, K.; Shen, Q.; Iikubo, S.; Minemoto, T.; Yoshino, K.; Hayase, S. Lead-free tin-halide perovskite solar cells with 13% efficiency. *Nano Energy* 2020, 74, 104858.
75. Chen, L.-J.; Lee, C.-R.; Chuang, Y.-J.; Wu, Z.-H.; Chen, C. Synthesis and Optical Properties of Lead-Free Cesium Tin Halide Perovskite Quantum Rods with High-Performance Solar Cell Application. *J. Phys. Chem. Lett.* 2016, 7, 5028–5035.
76. Fan, Z.; Sun, K.; Wang, J. Perovskites for photovoltaics: A combined review of organic–inorganic halide perovskites and ferroelectric oxide perovskites. *J. Mater. Chem. A* 2015, 3, 18809–18828.
77. Cao, J.; Yan, F. Recent progress in tin-based perovskite solar cells. *Energy Environ. Sci.* 2021, 14, 1286–1325.
78. Krishnamoorthy, T.; Ding, H.; Yan, C.; Leong, W.L.; Baikie, T.; Zhang, Z.; Sherburne, M.; Li, S.; Asta, M.; Mathews, N.; et al. Lead-free germanium iodide perovskite materials for photovoltaic applications. *J. Mater. Chem. A* 2015, 3, 23829–23832.
79. Liu, Y. The development of low toxic and high efficient solar cells. *J. Phys. Conf. Ser.* 2020, 1653, 12002.

80. Kopacic, I.; Friesenbichler, B.; Hoefler, S.F.; Kunert, B.; Plank, H.; Rath, T.; Trimmel, G. Enhanced Performance of Germanium Halide Perovskite Solar Cells through Compositional Engineering. *ACS Appl. Energy Mater.* 2018, 1, 343–347.
81. Chen, M.; Ju, M.-G.; Garces, H.F.; Carl, A.D.; Ono, L.K.; Hawash, Z.; Zhang, Y.; Shen, T.; Qi, Y.; Grimm, R.L.; et al. Highly stable and efficient all-inorganic lead-free perovskite solar cells with native-oxide passivation. *Nat. Commun.* 2019, 10, 16.
82. Öz, S.; Hebig, J.-C.; Jung, E.; Singh, T.; Lepcha, A.; Olthof, S.; Jan, F.; Gao, Y.; German, R.; van Loosdrecht, P.H.M.; et al. Zero-dimensional (CH<sub>3</sub>NH<sub>3</sub>)<sub>3</sub>Bi<sub>2</sub>I<sub>9</sub> perovskite for optoelectronic applications. *Sol. Energy Mater. Sol. Cells* 2016, 158, 195–201.
83. Hu, W.; He, X.; Fang, Z.; Lian, W.; Shang, Y.; Li, X.; Zhou, W.; Zhang, M.; Chen, T.; Lu, Y.; et al. Bulk heterojunction gifts bismuth-based lead-free perovskite solar cells with record efficiency. *Nano Energy* 2020, 68, 104362.
84. Yang, Y.; Liu, C.; Cai, M.; Liao, Y.; Ding, Y.; Ma, S.; Liu, X.; Guli, M.; Dai, S.; Nazeeruddin, M.K. Dimension-Controlled Growth of Antimony-Based Perovskite-like Halides for Lead-Free and Semitransparent Photovoltaics. *ACS Appl. Mater. Interfaces* 2020, 12, 17062–17069.
85. Elseman, A.M.; Shalan, A.E.; Sajid, S.; Rashad, M.M.; Hassan, A.M.; Li, M. Copper-Substituted Lead Perovskite Materials Constructed with Different Halides for Working (CH<sub>3</sub>NH<sub>3</sub>)<sub>2</sub>CuX<sub>4</sub>-Based Perovskite Solar Cells from Experimental and Theoretical View. *ACS Appl. Mater. Interfaces* 2018, 10, 11699–11707.

---

Retrieved from <https://encyclopedia.pub/entry/history/show/25011>